Journal of Industrial and Engineering Chemistry xxx (xxxx) xxx

Contents lists available at ScienceDirect

Journal of Industrial and Engineering Chemistry

journal homepage: www.elsevier.com/locate/jiec

Photochromic photography with hackmanite obtained by large-scale synthesis

Sami Vuori [a,b], Hannah Byron [a,b], Isabella Norrbo [a], Minnea Tuomisto [a], Mika Lastusaari [a,*]

[a] Department of Chemistry, University of Turku, FI-20014 Turku, Finland
[b] University of Turku Graduate School (UTUGS), Doctoral Programme in Exact Sciences (EXACTUS), FI-20014 Turku, Finland

ARTICLE INFO

Article history:
Received 18 October 2022
Revised 16 December 2022
Accepted 25 December 2022
Available online xxxx

Keywords:
Film photography
Tenebrescence
Photochromism
Hackmanite

ABSTRACT

Hackmanite ($Na_8Al_6Si_6O_{24}(Cl,S)_2$) is an intelligent mineral that changes its color from white to pink upon exposure to UV radiation, X-rays, or gamma radiation and reverts to white by exposure to visible light or heat. This reversible photochromism can be used in e.g. solar UV indexing, X-ray imaging, gamma radiation detection, and intelligent clothing. Hackmanite is conventionally synthesized in a laboratory with yields measured in grams, which is low in an industrial aspect when considering the material's vast application portfolio. In this work, we show that it is possible to produce hackmanite in an industrial scale with the final product yield of up to 1 kg marking a significant advance towards the commercial use of hackmanite. We also show yet another novel application invention: a photochromic photographic film that can be reused indefinitely due to hackmanite's coloration ability that does not weaken with repeated use.

Introduction

Hackmanite, also known as photochromic sodalite, is a natural mineral found in e.g. Greenland, Pakistan, Afghanistan, Canada, and Russia [1,2]. It is an intelligent mineral showing optical properties such as purple or pink tenebrescence i.e. photochromism, fluorescence, photoluminescence, and persistent luminescence upon exposure to UV light and has been a scientific interest for almost a century [3–6]. Since natural hackmanite is rare, extracting it is difficult and costly, and it has impurities that cannot be controlled [7], laboratory synthesis is a preferred method when materials with controlled and predictable properties are required. Owing to such control, it has been previously shown that hackmanite's color-changing properties can be employed in the indication of solar UV indexing [8], X-ray imaging [9] as well as nuclear radiation mapping and dosimetry [10]. Furthermore, hackmanite can "remember" previous exposure to high-energy radiation such as alpha and gamma by a subtle change in its reflectance spectrum. This is referred to as "gamma memory" [10]. In the present work, we show that hackmanite can even be used to make reusable non-toxic film for regular photography.

Successful hackmanite synthesis routes that have been reported in literature are microwave, solid-state, and hydrothermal [4,8,11–16]. The laboratory-scale solid-state synthesis is conventionally conducted in an alumina boat or a crucible in a high-temperature furnace, usually yielding only up to 10 grams of material per batch [8,9,12,17]. However, for any commercial use, such batches are too small. Nonetheless, industrial-scale syntheses have not been reported earlier. We present results of an upscaled synthesis method yielding up to 1-kg hackmanite batches made in an industrial retort furnace designed mainly for quenching of steel alloys [18]. The overall synthesis procedure is rather rudimentary and requires no delicate or labor-intensive steps, which is beneficial to the purpose of synthesizing hackmanite quickly and easily on a larger scale.

In terms of reversible photochromism, some recently-discovered materials are e.g. $Sr_3YNa(PO_4)_3F:Eu^{2+}$ (absorption maxima at 450 and 596 nm) [19], $Na_{0.5}Bi_{2.5}Nb_2O_9$:Sm (458 nm) [20], $Mg_4Ga_8Ge_2O_{20}:Cr^{3+}$ (480 nm) [21], $KSr_2Nb_5O_{15}$ (532 and 689 nm) [22], $BaMgSiO_4$ (520 nm) [23,24] and $Sr_3GdNa(PO_4)_3F:Eu^{2+}$ (606 nm) [25]. The coloration depth, bleaching, and reversibility are in a range and at levels where they could be used in various practical applications regarding photochromism, yet they share the disadvantage of being composed of toxic, scarce and/or expensive elements [26]. Hackmanite, however, has a target compositional formula $Na_8Al_6Si_6O_8(Cl,S)_2$, which shows that it contains

* Corresponding author.
E-mail address: miklas@utu.fi (M. Lastusaari).

https://doi.org/10.1016/j.jiec.2022.12.043

Please cite this article as: S. Vuori, H. Byron, I. Norrbo et al., Photochromic photography with hackmanite obtained by large-scale synthesis, Journal of Industrial and Engineering Chemistry, https://doi.org/10.1016/j.jiec.2022.12.043

only non-toxic and abundant elements, rendering it a sustainable material and because of its immediate (fluorescence, photoluminescence and photochromism) and latent (persistent luminescence) reactions to its surroundings, it can be considered an intelligent material. Hackmanite is all the more interesting because of the indefinite reversibility and rechargeability of the material, meaning that like the other optical properties, the tenebrescence also does not weaken with repeated use [27]. Our work focuses more on the photochromic aspect, which has been reported to occur upon UV, X-ray, alpha, beta, electron, positron, and gamma exposure [4,9,10,14–16]. The material's response to high-energy photons to produce an easily observable and measurable coloration is of particular interest since hackmanite falls in the category of reusable and non-toxic materials, whereas the majority of the currently used dosimeters and other radiation detectors do not [10]. Hackmanite has a growing portfolio of potential applications: tenebrescence imaging with X-rays or gamma [9,10], leisure applications such as mixing hackmanite with cellulose fibers to manufacture clothes that react to UV radiation [17], or as the key component in a UV index meter [8]. This increases the demand for production on a larger scale than is possible in a laboratory.

Hackmanite's reversible coloration is based on lattice defects that are chloride vacancy (V_{Cl}) and disulfide (S_2^{2-}) ion pair systems, where electrons are excited from the latter with photons that have enough energy to excite the disulfides's valence electron that eventually lands in the V_{Cl} trap. After this transition has occurred, the formed color center (F center) absorbs visible light, with the absorption maximum located at ~540 nm (green part of the visible spectrum), making the material's observed color appear pink. During the creation of the color center there is subtle atomic reorganization near the color center, but no chemical bonds are broken during this process. This allows reversion of the atomic structure to its original state with little energy, which in this case is visible light or heat. This property is responsible for the coloration and bleaching, which can both be induced indefinitely. [7,8,27,28] A more detailed description about the mechanism and mechanics of the photochromism is presented later in the text.

We present a method to make industrial-scale batches of phase-pure synthetic hackmanite powder that can then be used as prepared or cast as a film or used in a way where the hackmanite crystals can be colored with radiation, and the coloration can then be read with a spectrometer, a camera, or other methods. We also show a new application related to the tenebrescence feature: in this work, hackmanite is used as a photographic film by mixing it with organic and silicone film media that hold the particles in place, while still maintaining flexibility and durability. The films are then used and exposed like conventional photographic film with an exposable size of 6 × 6 cm.

Experimental

Synthesis

Two batches of hackmanite were prepared: 1 kg and 100 g. When making the former, one kilogram of starting materials was weighed with a Radwag PS 1200/C/2 precision balance and mixed by simply pouring the reagents into a 2-litre plastic ziplock bag and shaking and turning the bag for 5 minutes by hand. The weighed amounts were 700 g of zeolite A (Sigma Aldrich, dried at 500 °C for 1 h prior to weighing in a Nabertherm N3/C8 furnace), 240 g of NaCl powder crushed from crystals (>99.5%, J. T. Baker), and 60 g of Na_2SO_4 (Merck, > 99%), a recipe introduced by Armstrong et al [15]. For the synthesis of this large an amount, a custom container was made using common crafts clay ("267 vaalea/keltainen AR-267 koulusavi 0–0,2 mm samotilla", Kerasil product number 525205), seen in Fig. 2. After the initial hand-molding process, the container was dried in a Termaks TS 8024 incubator at 65 °C for 4 h with fan speed 1. After this, the inner lining of the container was coated with Cotronics Resbond® 989 aluminum oxide paste to minimize the clay minerals' leeching into the hackmanite material. After 24 h drying in room temperature, the container was fired in a Thermolyne F30400 furnace in air at 975 °C for 1 h with a ramp rate of 18 °C/min to convert the raw clay into a ceramic. After the heating, the furnace was let to cool passively to room temperature overnight.

The hackmanite precursor mixture was poured from the ziplock bag into the clay container, which was then heated in a Thermolyne F30400 furnace at 850 °C for 2 h (ramp rate 18 °C/min) and let to cool passively to room temperature overnight. The product was then taken out of the container to a plastic bag and simply crushed with a mallet and put into the container again. Then the container was lowered to the bottom of a steel-lined heavy-duty retort furnace (Fig. 1a and b) with an inner volume of 1.36 m^3 in Hilamet Oy, Ylihärmä, Finland. The furnace was flushed by letting 2.5 m^3 of FORMIER® 10 gas (H_2 12% / N_2 88%, gas bottle volume 50 l) mixture flow through it with a flow rate of ~83 l/min (calculated from the bottle's pressure drop from 200 to 150 bar in 30 minutes) at normal temperature and pressure. After this, the gas flow rate was decreased to 1.0 l/min (measured with Kytölä Instrumentit serial no 101,972 rotameter set to 150) and the heating was started. The dwell temperature was set to 850 °C, dwell time to 2 h and the ramp rate to 10 °C/min. After the heating step, the furnace was let to cool down passively for 20 h, after which it had reached a temperature of 200 °C. The gas flow was cut off and the sample was removed from the furnace. This sample was named "Hack 1 kg". The whole synthesis procedure including washing is depicted in Fig. 1c.

When the 1 kg batch was inspected in the laboratory with UV lamps, initial observations of the sample were that the surface layer had reduced luminescent properties (Fig. 2), but after removing ~1 cm from the sample (overall thickness ~5 cm), the underlying bulk showed luminescence, afterglow, and tenebrescence, as is shown later.

Another batch of hackmanite was later synthesized using 100 g of the same starting materials as in "Hack 1 kg" but scaled 10 times smaller (70 g zeolite A, 24 g of NaCl crushed into powder, and 6 g of Na_2SO_4). The synthesis procedure was kept the same, but the only difference in the conditions was that the container had a lid to protect the sample from the contaminating metal particles chipping off the inner parts of the furnace, as was observed with the 1 kg batch. The container also had grooves to let the gas flow freely into the sample (Fig. 3). This sample was named "Hack 100 g".

Analysis methods

The purity and optical properties of the samples were investigated with X-ray powder diffraction, X-ray fluorescence, luminescence spectrometry, and reflectance spectrometry. From both Hack 1 kg and Hack 100 g, 19 aliquots were collected from different places in the sample shown and analyzed separately to gain information about the variation of the purity and tenebrescence properties within the large sample mass.

X-ray diffraction measurements were conducted with PANalytical Aeris operating at 40.0 kV and 7.5 mA with PIXcel1D-Medipix3 detector and using Cu $K_{\alpha 1,2}$ radiation with 1/2° divergence slit, 13 mm mask, 0.04 rad soller slits, 9 mm anti-scatter slit, nickel beta-filter, high beam knife, 1 rps spinner speed and using a scan rate of 0.201 °/s with a step size of 0.0217°. Rietveld refinements were conducted for the unit cell parameters and scale factors in PANalytical HighScore Plus 4.9.0.27512 by determining the background with a bending factor of 2 and granularity 20 using

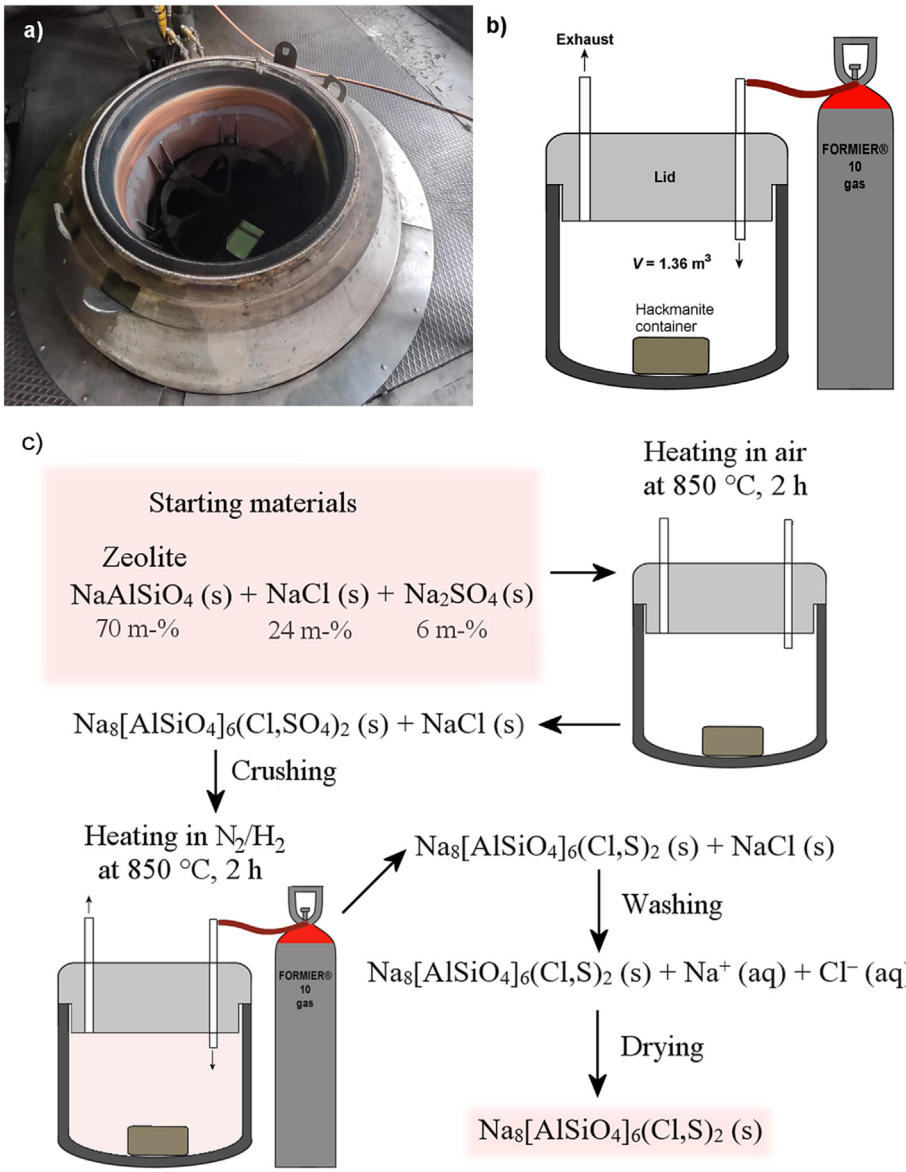

Fig. 1. A) the retort furnace open, showing the 1-kg hackmanite precursor mixture at the bottom of the retort furnace before synthesis. b) schematics of the retort furnace when closed. when the furnace is closed, the inner empty volume is 1.36 m^3. Prior to starting the synthesis procedure, the furnace was first flushed with 2.5 m^3 of FORMIER® 10 gas which was connected in the furnace throughout the whole synthesis with a flow rate of 1.0 l/min. c) Hackmanite's synthetic scheme used in this work, from the starting materials to a washed product.

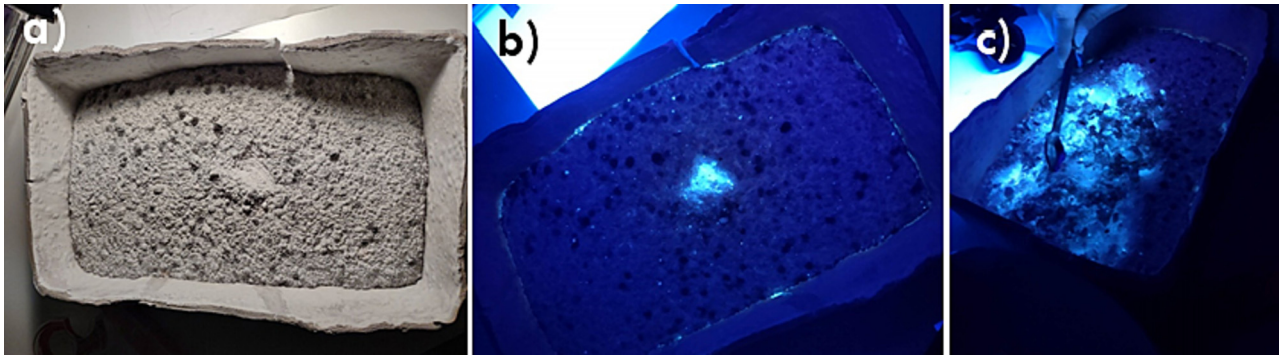

Fig. 2. The Hack 1 kg batch after the reduction a) under a 60-W incandescent light, some dark particles from the furnace can be seen on the surface b) under 302 nm UV lamp (UVP UVM-57 operating with 6 W) with a part of the surface layer removed in the middle, showing luminescent material below c) more of the surface removed, showing more luminescent material. The container's size is 30 × 17 × 10 cm.

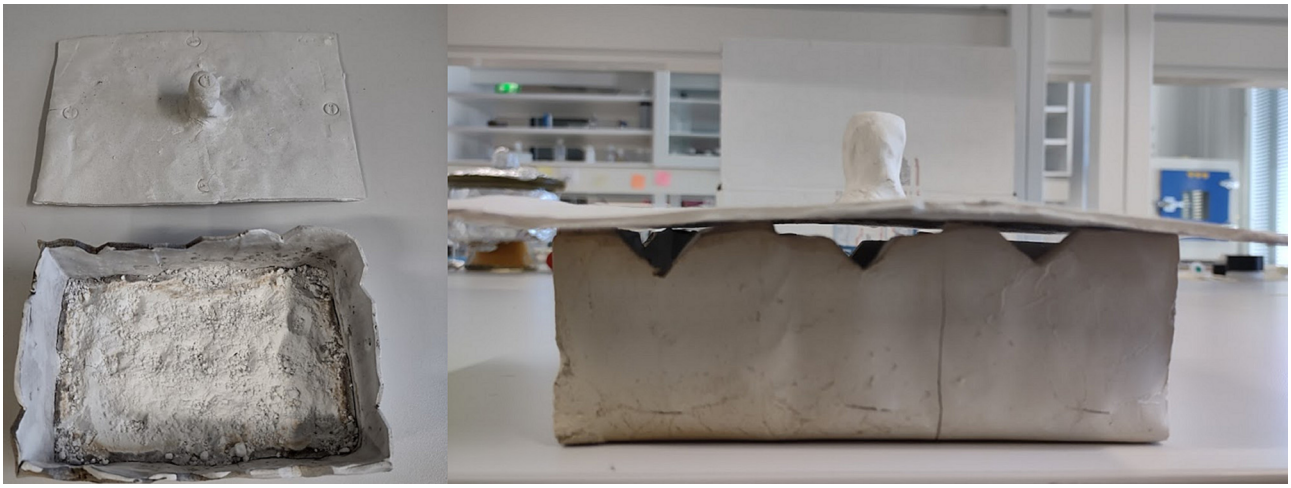

Fig. 3. The container for the 100 g hackmanite batch. Gas flow grooves can be seen in the sides. The container's size is 15 × 10 × 5 cm.

smoothed input data. Then, the peaks were searched with a minimum significance of 2.00, minimum tip width 0.01, maximum tip width 1.00, peak base width 2.00, method Minimum 2nd derivative. The search & match pattern list was used from a subset consisting of PDF-4+2021 4.21.0.2 (database version 4.2103) database occurrences 04-017-7136 ($Na_8Al_6Si_6O_{24}Cl_{1.8}S_{0.1}$) and 04-016-5475 (NaCl). Then, the peaks were fitted with HighScore's default profile fit and subsequently refined with default Rietveld using available background as the method in global variables.

Tenebrescence coloration tests of the finished 1 kg and 100 g batches were carried out with a Konica Minolta CM-2300d spectrometer. The samples were measured before and after exposure to 254 nm UV lamp (Analytikjena UVLS-24 254 nm 4 W) for 5 min, which translates to a UV fluence of 920 mJ/cm^2. The coloration value was determined as the integral of the difference between the two spectra, being a quantitative value with an arbitrary unit. The reflectance spectra of the non-colored and colored film were measured with Avantes AvaSpec HS-TEC using Avantes AvaLight-DHc as the light source and Avantes AvaSoft 8.11.0.0 as the measurement software in reflectance mode. The measurements were conducted by taking a white reference from a MgO powder (synthesized from $MgCO_3$; Merck 5827, p.a.; by heating at 1000 °C for 1 h in a Nabertherm N3/C8 furnace) and keeping the integration time at 500 ms with 5 averages per measurement. After measuring the non-colored form, the sample was colored with a 254 nm UV lamp (UVLS-24) for 5 minutes, after which the reflectance was measured immediately.

The tenebrescence excitation spectrum measurements were conducted by inducing coloration and bleaching with a Xe lamp (LOT-QuantumDesign LSB522, 150 W) with each wavelength chosen with a LOT-QuantumDesign MSH300 monochromator and measuring the color with Avantes AvaSpec HS-TEC using Avantes Ocean Optics LS-1-Cal as the light source and Avantes AvaSoft 8.11.0.0 as the measurement software in reflectance mode. The measurements were conducted by taking a white reference from a non-colored sample and keeping the integration time at 160 ms with 10 averages per measurement. Data points are integrals of spectra from 400-800 nm, with all spectra vertically aligned at 1000 nm using 20 averaging points and corrected for the monochromator lamp's emission intensity at each excitation wavelength. The tenebrescence fading curves' bleaching was calculated from reflectance spectra integrals from 400-750 nm, with all spectra vertically aligned at 1000 nm using 20 averaging points and corrected for spontaneous fading in darkness. Irradiation time for both excitation and fading spectra was 5 min.

The Hurter–Driffield curves were obtained by using an Avantes AvaSpec 2048–14 spectrometer in reflectance mode in Avantes AvaSoft 8.11.0.0 and taking a white reference from the sample in its non-colored form, then coloring the hackmanite type with a 9-W 254 nm UV lamp (model 博立恩ZW9D12W-H145) for 5 min and letting it fade spontaneously in darkness for 24 h in order to minimize the effect of spontaneous fading on the results (more information in Fig. S6) and finally measuring its reflectance spectra for 10 h (powder and silicone film) or 5.4 h (organic film) under a 120-W halogen lamp producing 23,000 lux at the measurement spot.

Luminescence spectra were measured with Varian Cary Eclipse fluorescence spectrometer (software Cary Eclipse Scan Application 1.2(147)) in Phosphorescence mode with total decay time of 0.0051 s, delay time 0.1 ms, gate time 5.0 ms, number of flashes 1, excitation slit 10 nm, emission slit 2.5 nm, data interval 0.2000 nm, delay time 0.0050 s and PMT voltage 800 V (high). The persistent luminescence spectra were collected by exciting the sample for 5 minutes with a UV lamp (Analytikjena UVLS-24 254 nm, 4 W and Analytikjena UVM-57 302 nm, 6 W), then waiting for 15 s before collecting the spectra in Bio-/chemiluminescence mode with parameters emission slit 20 nm, data interval 1.0000 nm and PMT voltage 800 V (high). The luminance fading curves were obtained by exciting the sample for 5 minutes with a UV lamp (Analytikjena UVLS-24 254 nm, 4 W and Analytikjena UVM-57 302 nm, 6 W), then waiting for 15 s and collecting the signal in 1-second intervals with Hagner ERP-105 photopic luminance meter with Hagner Detector SD-27 coupled to a Fluke 189 multimeter, the control software being FlukeView® Forms v3.8.0003, 2014. The thermoluminescence measurements were obtained by exciting the sample for 5 minutes with a UV lamp (Analytikjena UVLS-24 254 nm, 4 W), then waiting for 1 min before starting the measurement with Mikrolab Laboratory Reader-Analyser RA'04 (software Mikrolab, TLD Reader/Analyser v0.9.401, 2001). The heating parameters were set to test: 1750, heat rate: 10.0 °C/s, max temp: 400.0 °C, temp 1: 40.0 °C, temp 2: 265.0 °C, temp 3: 400.0 °C, time 1: 1.00 s, time 2: 1.00 s, time 3: 1.00 s, time test: 10.00 s, time BKGN: 60.00 s, ACOMP-M: 4, ACOMP-T: 8.

Films

For the photochromic photography application, two types of films were cast using hackmanite. The first type was made by mixing 20 m-% of hackmanite with Dow SYLGARD™ 184 silicone elastomer kit (consisting of 10 m-% of curing agent and 90 m-% of silicone base). The hackmanite powder was first sieved through a 25 μm sieve, then mixed with the silicone elastomer and applied

onto a 0.1-mm thick Folex® Premium Universal Copy Film X-100 A4 (art no. 39100.100.44000) polyethylene film. Then the mixture was deaerated in a Memmert VO 200 vacuum oven at 25 °C and 10 mbar for 10 minutes, after which it was cast as a 300-µm thick tape with an Erichsen Coatmaster 510 film applicator and cured at 60 °C for 1 h in a Termaks TS 8024 incubator with fan speed 1.

Another hackmanite film was based on a flexible tape which is cast using a slightly modified process that was presented by Abhinay et al [29]: the mixture of 40 m-% hackmanite, 30 m-% 2-butanone, 15 m-% ethanol, 2 m-% Triton X-100, 7 m-% polyvinyl butyral, and 6 m-% benzyl butyl phthalate is mixed in a ball mill (Philips Minimill PW4018/00 at speed 1 for 10 min when mixing hackmanite powder, 2-butanone, ethanol, and Triton X-100, and subsequently at speed 5 for 2 minutes when mixing the remaining reagents) and cast as a 300-µm thick tape with an Erichsen Coatmaster 510 film applicator onto a 0.1-mm thick Folex® Premium Universal Copy Film X-100 A4 (art no. 39100.100.44000) polyethylene film. After the evaporation of 2-butanone and ethanol, the film's thickness is 117 µm (Fig. S12) and consists of roughly 73 m-% of hackmanite powder, the rest being polyvinyl butyral (13 m-%), benzyl butyl phthalate (11 m-%), and Triton X-100 (3 m-%). This formulation allows the film to be flexible and wear resistant.

When taking a photograph, the film is first colored with UV light. For this purpose, the 9-W 254 nm lamp (acquired for a minimal $7) was used. The film measuring 6 × 9 cm was exposed to UV light for 5 minutes, after which it had the hackmanite's characteristic deep pink hue and was fully colored. The colored film was exposed with a VEB KWT Reflekta II camera with a Meritar *f*/3.5 75 mm lens for 20 h and then scanned with a household Canon CanoScan 5600F scanner.

Purification

Purification of the samples was conducted to see whether it influences optical properties. As will be shown later, the main impurity in finished hackmanite is unreacted, excess sodium chloride, which – as a water-soluble and hygroscopic mineral – may decrease the shelf life and performance of hackmanite-based products.

A part of the Hack 100 g batch was washed with deionized water to inspect the removal of excess NaCl and the effect on its optical performance after washing. 1.500 g of hackmanite from this batch was divided into five Eppendorf tubes, after which the first one was washed once with 1.000 ml of deionized water, the second two times, the third three times etc. In the washing procedure, the Eppendorf tube was shaken with a laboratory vortex for 15 s and then put into a centrifuge for 1 minute at 5000 g. Then, each of the supernatants were collected with a pipette into another Eppendorf tube and analyzed with XRF to determine the NaCl and hackmanite content. The washed hackmanite samples were put into an oven for 4 h at 100 °C to remove water from the samples and measured with XRD, and their optical properties were investigated with luminescence and reflectance spectrometry.

The amounts of Cl and Si were calculated by integrating the XRF's Cl and Si peaks and comparing them with a standard series that were made using NaCl and SiO_2 (Fig. S7).

Results

Purity and intra-batch variation

The purity and the depth of UV-induced tenebrescence of the 1 kg and 100 g batches are shown in Fig. 4. The coloration depth is clearly highest in the center part of the container, meaning that the center part was reduced the best, while the edges suffer from decreased ability to color. This may be due to leeched clay minerals from the container's surface or poor permeability of the reducing gas. The purity, measured as excess NaCl content analyzed from XRD data by Rietveld refinement shows that in Hack 1 kg the purity varies from region to region, as does Hack 100 g's, yet the latter's overall purity is higher. It is clear that in terms of purity and coloration depth, Hack 100 g was superior in both qualities, suggesting that using a lid is beneficial to the desired properties.

The XRD diffractograms from the combined 19 aliquots in Hack 1 kg and Hack 100 g (Fig. 5) show that the phase purity is high, and there is little excess NaCl left. Rietveld-refined average values of NaCl are 9.1% in Hack 100 g and 11.7% in Hack 1 kg, thus Hack 100 g's synthesis was more complete.

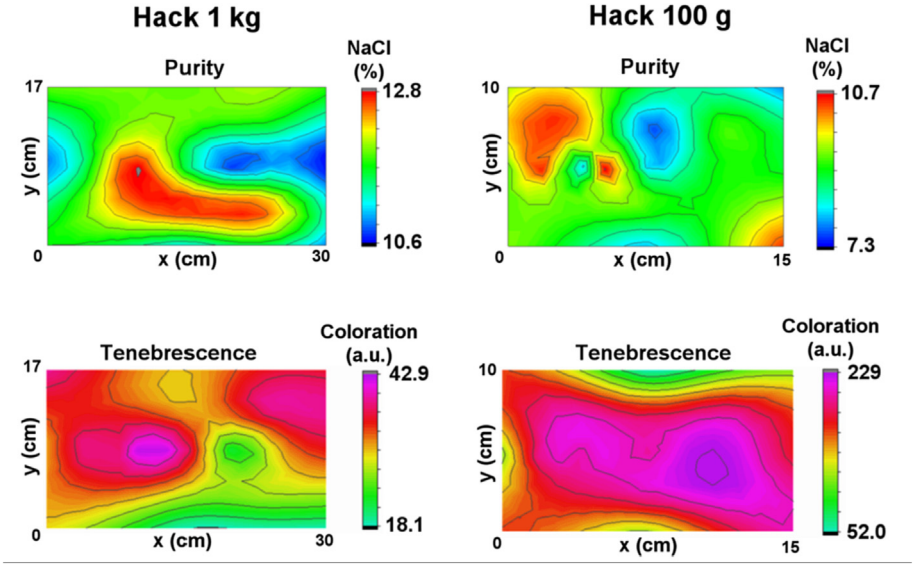

Fig. 4. 2D maps of purity and tenebrescence of Hack 1 kg and Hack 100 g made from measurements taken from 19 different locations in the synthesis vessels. The figures show the sizes of the synthesis vessels in cm in x and y directions. In purity, lower NaCl content (blue) is advantageous, whereas in tenebrescence, higher coloration (pink) is advantageous.

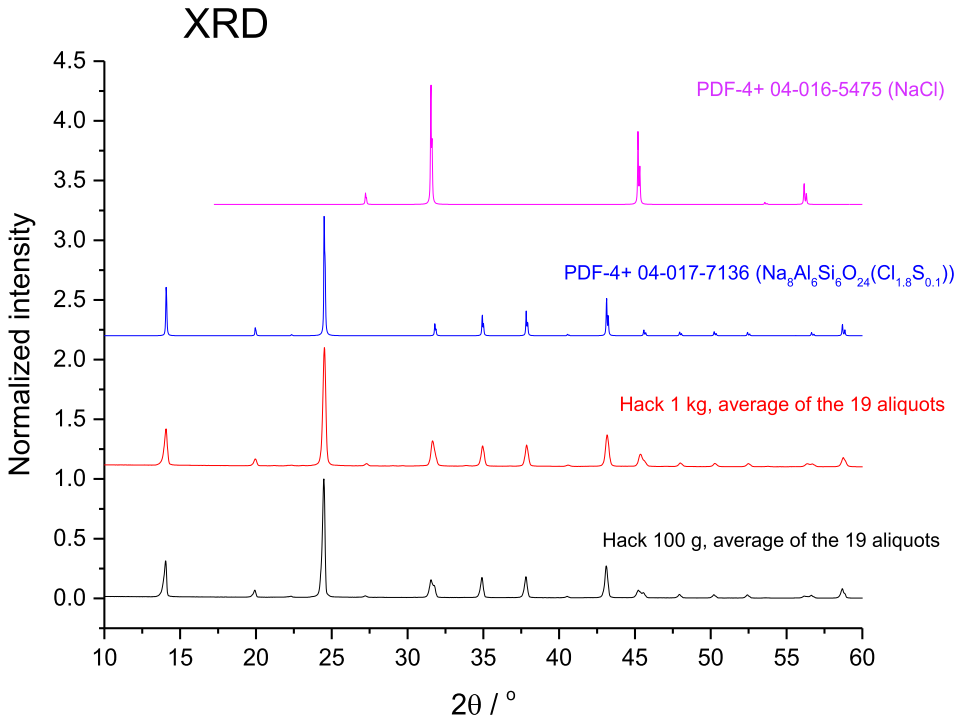

Fig. 5. X-ray diffractograms of the 100 g and 1 kg batches of hackmanite. The individual diffractograms are averages of the 19 aliquots. Rietveld-refined values of NaCl are 9.1% in Hack 100 g and 11.7% in Hack 1 kg.

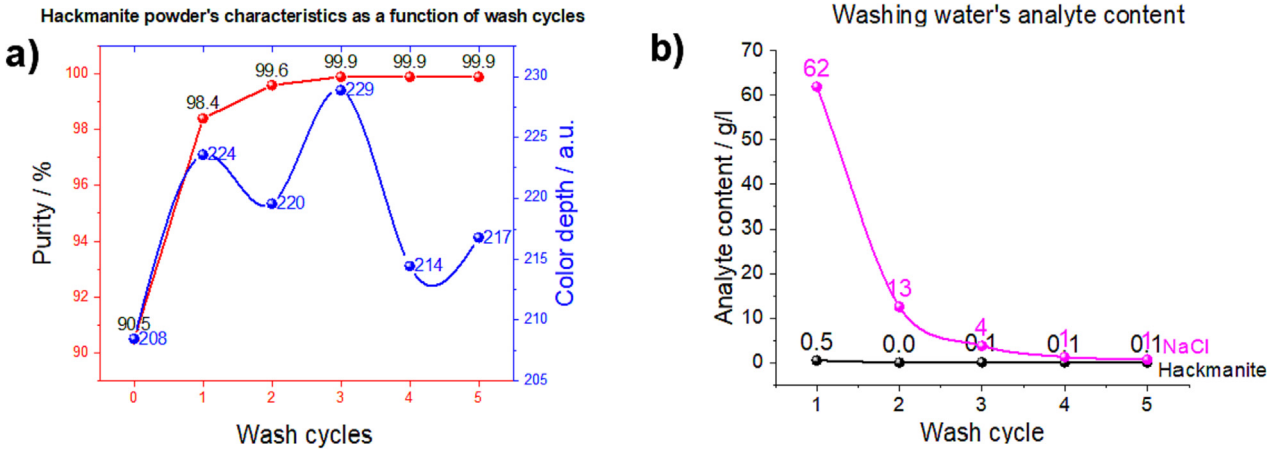

Fig. 6. a) The hackmanite powder's characteristics as a function of washing cycles. The purity was determined with Rietveld refinements, showing increasing relative hackmanite content by subsequent washing cycles, which in turn translates to less unreacted NaCl and thus higher purity. The coloration ability (Color depth) is unaffected by the washes as it stays at a rather constant value with only a ±5% variance. b) The washing water's analyte content as a function of wash cycles showing that with each successive washing cycle the amount of NaCl decreases, meaning that NaCl dissolves well in the water. The X-ray diffractograms of the samples from different parts of the washing procedure are presented in Fig. S8.

The effect of washing on purity and optical properties was investigated with Hack 100 g and the results are presented in Fig. 6. The hackmanite powder's purity increases asymptotically until the third wash where it plateaus at 99.9%, without affecting negatively to the coloration (Fig. 6a). The washing water's NaCl content is the highest after the first wash (Fig. 6b) and decreases rapidly and behaves conjointly with the purity level analysed by Rietveld refinements. The disadvantageous hackmanite leeching is highest after the first wash, but is very low since hackmanite, being essentially a material with a zeolitic structure, is not a water-soluble mineral [30]. In conclusion, it is most profitable to stop the washing at the third cycle. The total required amount of pure water for the three-cycle purification is only 12 litres per 1 kg of hackmanite, and when thinking sustainably, the dissolved NaCl can be regained from the water by evaporation and used for the next batch.

When the purification is complete, hackmanite has very little unreacted NaCl. The salt could shorten the life of the product due to its hygroscopic nature, especially as a fine powder with a large total surface area.

The effect of iron on luminescence properties

Iron is a known luminescence quencher [7,31], and as the Hack 1 kg sample had weaker luminescent properties on the surface, Fe contents in the samples were measured with XRF to gain informa-

tion about the correlation between the impurity and luminescence. Hack 1 kg's surface layer and the underlying bulk material were measured separately but Hack 100 g's sample consisted of both the bulk and the surface since the hackmanite layer itself was too thin to separate the two. Fig. 7 shows that the Hack 1 kg's surface contains over twice as much Fe than the bulk, whereas Hack 100 g contains slightly more Fe than the Hack 1 kg bulk. The Hack 100 g's container's lid hindered the Fe contamination of the sample from the furnace, and in Hack 1 kg the surface layer acted as a protective layer for the bulk material. This indicates that protecting hackmanite during the synthesis with a lid is an advantageous addition to the setup.

The luminescence properties of the Hack 100 g surface + bulk, Hack 1 kg bulk, and Hack 1 kg surface layer samples were characterized by measuring luminescence spectra (Fig. S2), persistent luminescence spectra (Fig. S3), thermoluminescence curves (Fig. S4) and luminance fading curves (Fig. S5). The data shows that, as presented in Fig. 2 and Fig. 8, the luminescence properties are severely quenched in the Hack 1 kg surface layer, whereas the Hack 1 kg bulk has superior luminescence properties compared to others. The other visible properties are also presented in Fig. 8.

In Fig. 8 it is evident that Hack 100 g has the best photochromic coloration after 254 nm irradiation, whereas Hack 1 kg bulk's luminescent properties are superior. This could be because the more UV photons involved in the Ti^{3+}-V_O interaction responsible for luminescence [7,28], the less free photons are available to excite an electron from an S_2^{2-} ion to a V_{Cl}, which is the charge carrier trapping mechanism for tenebrescence [8,28]. In the Hack 1 kg surface sample both luminescence and tenebrescence are weak, most probably due to high Fe impurity content.

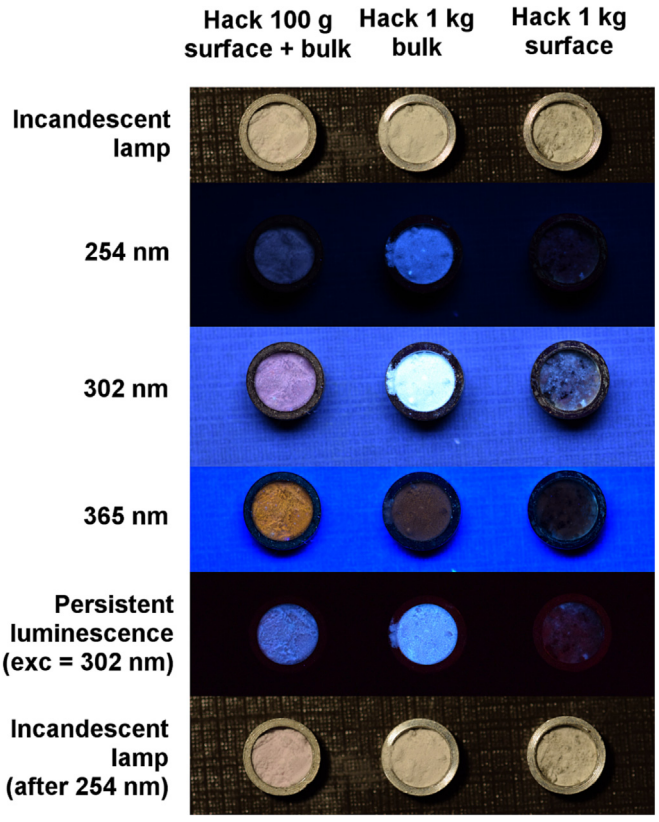

Fig. 8. Images of the samples Hack 100 g bulk + surface, Hack 1 kg bulk, and Hack 1 kg surface under various lighting conditions.

Application: Reusable photographic film

Although digital cameras and cellphones play the major part in capturing moments in everyday life, there is a resurgence of use of analog film by photography enthusiasts. It is still considered a niche due to rather low global demand, with prices having increased recently due to COVID-19, the global chip shortage, and environmental concerns, but due to a strong and dedicated user base, in 2021 Kodak reported an increased revenue on film sales of $8M (+12%) compared to 2020. [32] The problem with the current photographic films is that they are based on a silver halide emulsion that can be exposed only once, after which it must

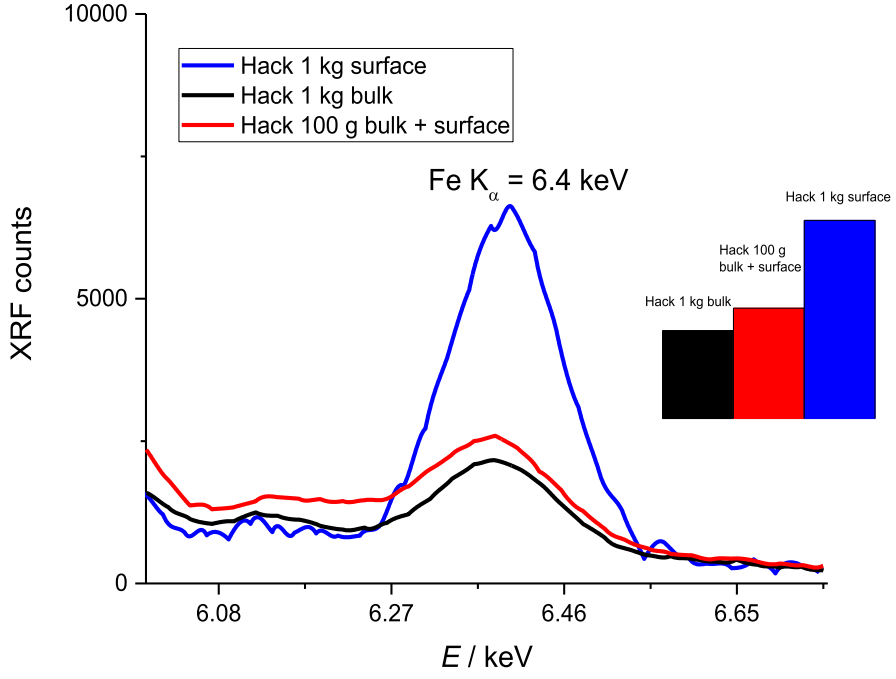

Fig. 7. X-ray fluorescence spectrum of Fe K_α showing that the Hack 1 kg's surface layer had an increased Fe content compared to Hack 100 g and Hack 1 kg bulk.

be developed with various chemicals (developer, stopper, and fixer). One more problematic aspect is that the film base uses animal-based gelatin. Although manufacturers have researched vegan alternatives for gelatin, they have not had success in replacing it. Gelatin not only works as a strong base layer for the silver halide particles but offers good permeability for development chemicals and dries fast [33], which is not needed in a hackmanite film.

In the present work, we show for the first time a hackmanite-based reusable, environmentally friendly photographic film that does not need a development process. The films are made with a well-colorable synthetic hackmanite sample made earlier in laboratory, yet the recipe is the same than in the large batches presented in this work.

While a silicone film mixed with 20% of hackmanite provides deep coloration and broad contrast region, initial tests showed that the image suffers from heavy Gaussian blur (Fig. 9) due to incident light scattering from the interfaces and in the silicone mass in the translucent material. It was then postulated that the organic film should not have this issue since it has a very high hackmanite content, providing an opaque layer where photon transmittance and scattering is minimal. This was confirmed by measuring the amount of transmitted light through the silicone (30%) and organic film (6.4%) (data shown in Fig. S9). The scattering was also tested by photographing the light leak with both film types: the scattering in the silicone film is 18% higher than in the organic film (Figs. S10 and S11).

Adjusting the hackmanite content in the silicone would improve its photographic performance, yet silicone elastomer becomes difficult to mix, deaerate, and cast with higher hackmanite concentrations, thus the organic film was used as the preferred photographic film in the subsequent tests.

The organic film's result can be seen in Fig. 10. It is clear that this film type outperforms the silicone one in clarity. It is noteworthy that the images seen here are not latent images and do not need any kind of developing after exposure has stopped, unlike conventional films.

The photograph was then erased by fully coloring the film again with the UV lamp, and the film was then used again to photograph new subjects (Fig. 11). The exposure time was kept at 20 h, but since lighting conditions in nature vary, the exposure results were different. Also, since hackmanite's spectral sensitivity curve for color fading peaks at green [9], color variation in the scene itself has an effect in the exposure. It seems that the left image is slightly underexposed, while the right image is slightly overexposed. The underexposed look can be explained by the red coloration of the

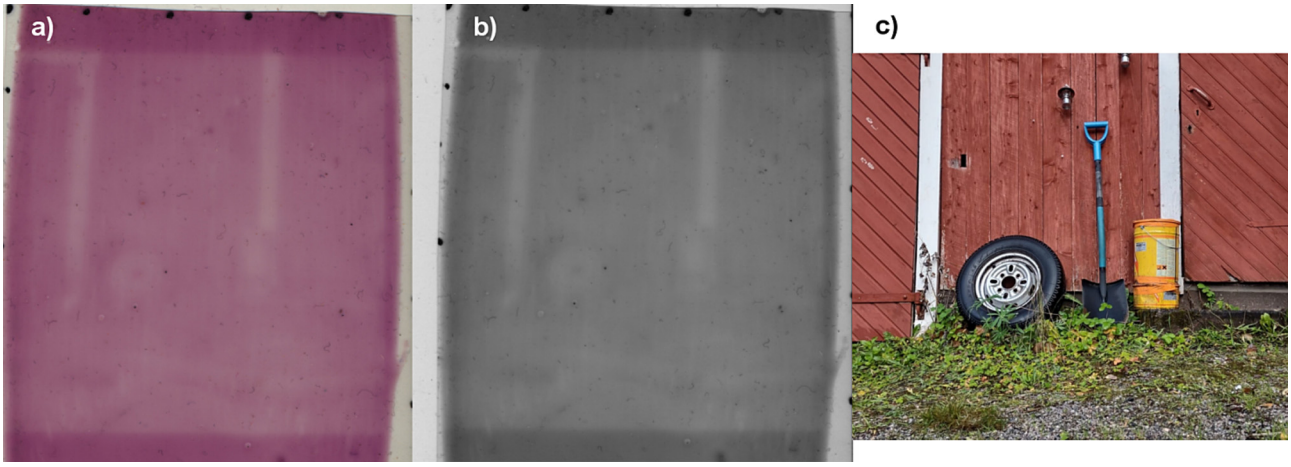

Fig. 9. The image taken with the silicone film. a) the film scanned after the 20-h exposure b) a greyscale conversion of the image c) the scene as it appears in reality. The image suffers from heavy Gaussian blur in spite of the camera lens being in focus.

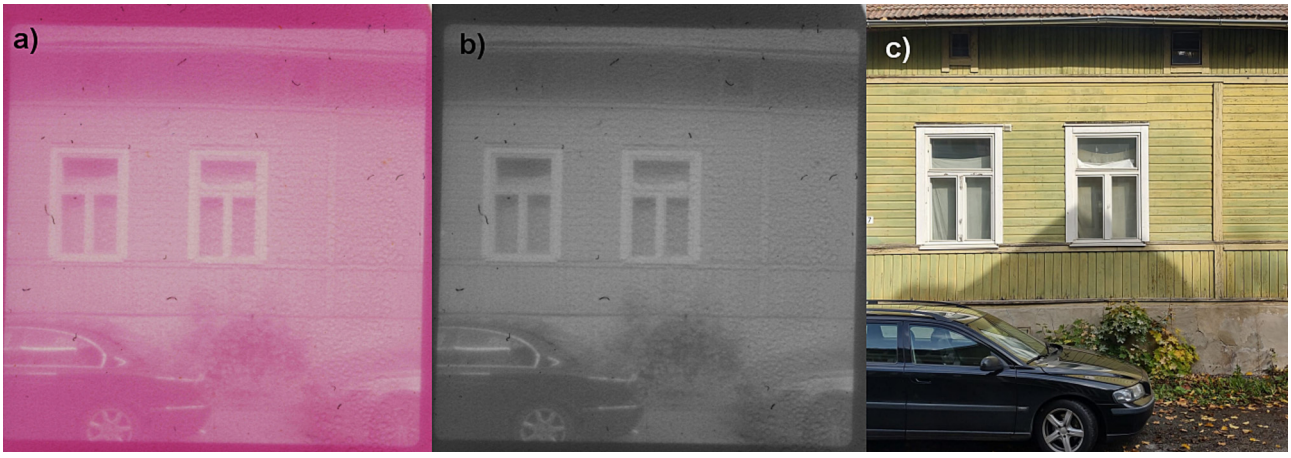

Fig. 10. The organic film used for photography. a) the film scanned after the 20-h exposure, b) the image converted to grayscale c) the scene as it appears in reality (image taken later, thus the scene has changed slightly).

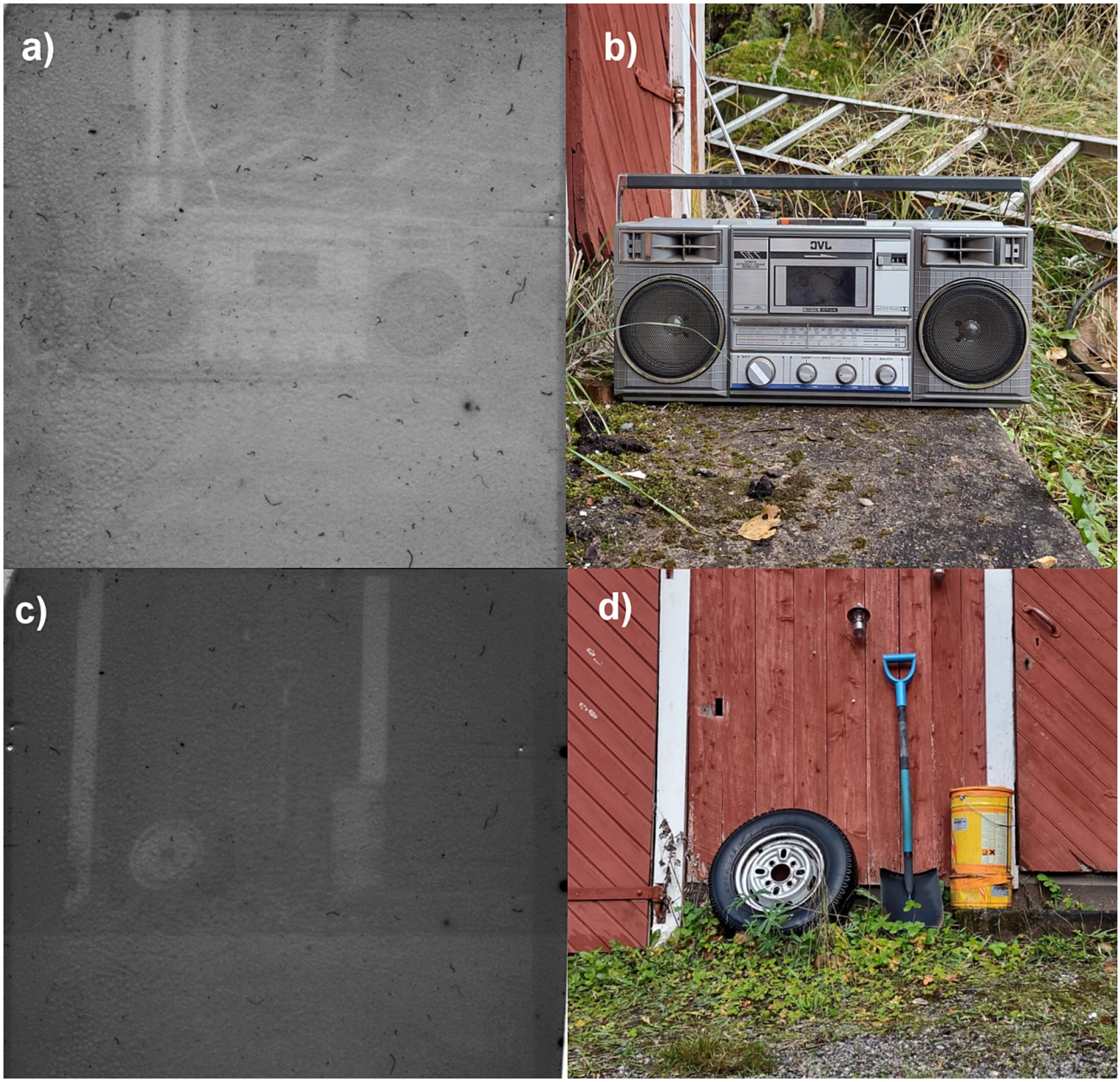

Fig. 11. Images taken with the organic film. a) a greyscale conversion of a 20-h exposure of a radio cassette player in the foreground, a ladder in the background b) the scene in reality c) a greyscale conversion of a 20-h exposure of a tire, a shovel and an oil barrel leaning against a red barn wall d) the scene in reality. N.B. the images suffer from increased dust particle buildup at each successive exposure due to handling in a home environment and scanning.

barn wall; while a photographic film made of hackmanite is panchromatic, different bleaching efficiencies of different wavelengths lead to red light bleaching (exposing in this case) hackmanite's coloration less effectively than green light, according to the material's bleaching spectrum (Fig. 13c and [8,14]).

Since the spontaneous fading of hackmanite does not progress after 24 h from the time of UV coloration (Fig. S6), the images can be archived in darkness indefinitely without losing any data.

For determining photographic film speed, performance, and correct exposure, constructing a sensitometric Hurter–Driffield curve is conventionally used. The four parts of the logistic curve are the toe (the underexposed part), the linear region (the usable exposure region), the shoulder (the overexposure region) and the last dip i.e. the region of solarisation. [34,35] Since conventional films with silver halide particles darken as a function of exposure, (higher exposure = higher absorbance), they are measured densitometrically, but the Hurter–Driffield curve of hackmanite can be constructed similarly using reflectance values from the bottom of the spectrum's valley, i.e. at 540 nm. The deeper the initial coloration is, the lower the value and vice versa. The $\times$ axis expresses exposure values logarithmically in conjunction with the fact that human senses perceive stimuli logarithmically, following the Weber–Fechner law described mathematically as $P = k \ln(s)$ where P = perception, k = a constant known as the Weber fraction which depends on the type of sense and stimulus and s = stimulus [36].

Hurter–Driffield curves of different hackmanite materials are presented in Fig. 12: a bare powder, a hackmanite film made of organic tape casting materials (organic film) and a silicone film. The curves in Fig. 12 show that the organic film has the faintest initial coloration but shows the response earliest. The linear region (contrast region) is rather narrow with the organic film, whereas silicone film shows deeper initial coloration and a broader contrast

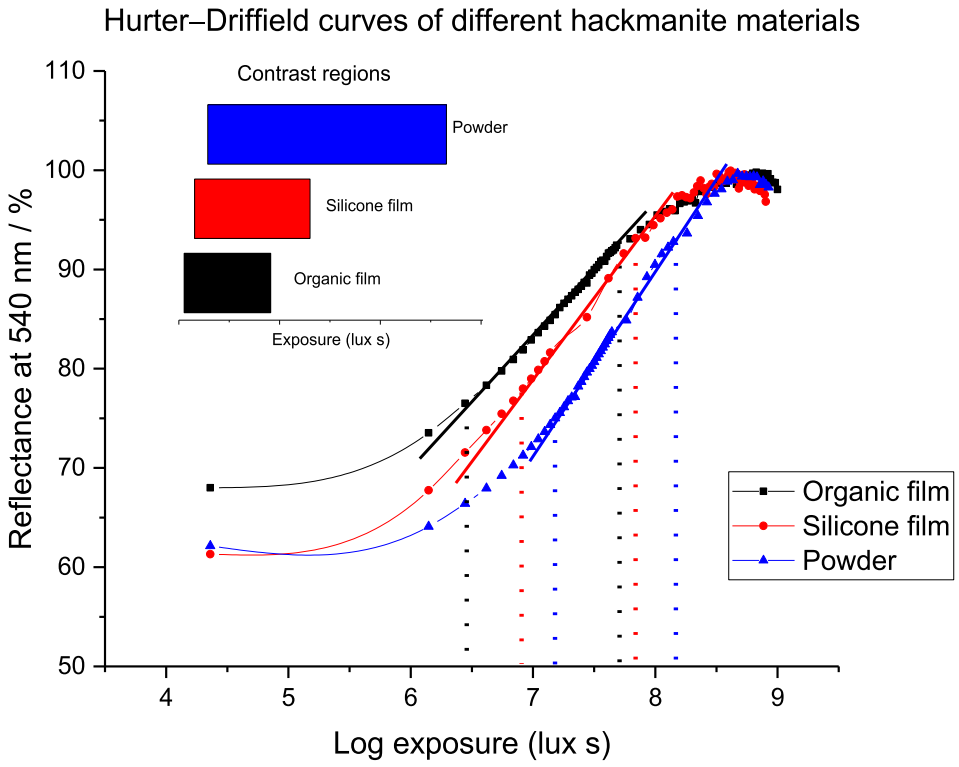

Fig. 12. Hurter–Driffield curves of an organic film (made of tape casting materials), silicone film and bare powder. The dotted lines show arbitrarily selected linear regions which mark the contrast limits. Inset: the contrast regions of Hurter–Driffield curves showing bare powder having the broadest one. Organic film is the fastest since it reaches the lower contrast limit with lowest exposure, whereas silicone film has a broader applicable range of the two films. The calculated gamma values (i.e. slopes of the linear region when both axes show logarithms of the measured values) of the curves are 0.0676 (organic film), 0.0832 (silicone film), and 0.0986 (powder). All curves' maxima are vertically aligned to the 100 % level.

region. The bare powder shows practically similar initial coloration depth with the silicone film but has a far broader contrast region than both films. Still, the films reach the contrast region with lower exposure than the powder, meaning that they are faster in imaging. On the other hand, the powder's broad contrast region renders it more forgiving in imaging: under- and overexposure is more difficult to achieve with bare powder. Still, bare powder is not an applicable form when considering a photographic film, meaning that a flexible film base must be used if the film is not used as a plate of pressed powder.

A standard 35 mm film has an exposure area of 24 mm × 36 mm and is prepared with 2 mm margins on each side, thus a 36-frame film roll has an exposable area of 32800 mm^2. When using 1 g of hackmanite to cast a 300-μm thick organic film, the film spreads to cover an area of 5900 mm^2 (Fig. S12). Thus, one 36-frame roll of organic hackmanite film would require 5.6 g of hackmanite, yet the actual amount would be higher due to mass losses in the casting procedure. In a medium format 120 film roll the operational area is 39000 mm^2 (56 mm × 56 mm · 12 exposures), requiring 6.6 g of hackmanite per roll. Thus, instead of normal laboratory-sized batches only the upscaled process fulfills the needs of photographic hackmanite film manufacture.

The mechanism and mechanics of photography with hackmanite

The backbone of the crystal structure of hackmanite is made up of corner-sharing AlO_4 and SiO_4 tetrahedra. These form a porous zeolitic 3D network of so-called sodalite cages, which incorporate Na_4Cl tetrahedra. [37] Since the pioneering works of Medved [4] and Kirk [6] in the 1950s, hackmanite's color change has been suggested to involve sulphur "impurity" species. By the 2000s, the consensus was that the sulphur species would probably be the disulfide ion (S_2^{2-}) replacing a few mole per cent of the chloride ions (Cl^-) [15]. Such aliovalent replacement results in the fact that for each replaced chloride ion, one empty chloride site (chloride vacancy, V_{Cl}) is also formed [16]. Fig. 13a shows the unit cell of hackmanite with one chloride replaced by disulfide.

With the maturation of computational methods in the late 2010s, it was possible to calculate the energy level schemes associated with the disulfide ions and the chloride vacancies [38]. Furthermore, experimental data confirmed these computational results [8] as well as the mechanism of color change suggested in the 2000s [15]. Enabled by the progress in computational methods, the most detailed view of the mechanism so far was presented in 2022 [27]. Below, we will present the details of the color change in hackmanites based on these earlier works.

The color change from white to any other color involves an electron transfer from the disulfide ion to the chloride vacancy [8,27,38]. This creates an excited S_2^--V_{Cl}^- pair, i.e. a color center, that absorbs visible light. For the present material, the absorption maximum is at 540 nm (2.3 eV) as shown in Fig. 13b. To clarify the energy needed to create the color center, we measured a tenebrescence excitation spectrum (Fig. 13c, right). It indicates that radiation in the range of 225–310 nm (4.0–5.5 eV) induces the coloration. The states involved in the mechanism as reported in [38] are presented in Fig. 13d.

The bleaching, i.e. returning to white, involves an electron transfer from the chloride vacancy back to the disulfide ion [8,27,38]. This process can be initiated by heating or by optical stimulation. In the present work, the optical stimulation process is used for the creation of the photographic image. Thus, we measured the tenebrescence bleaching spectrum for the hackmanite film (Fig. 13c, left), which suggests that color can be bleached with optical stimulation in the range of 355–689 nm (1.8–3.5 eV). The

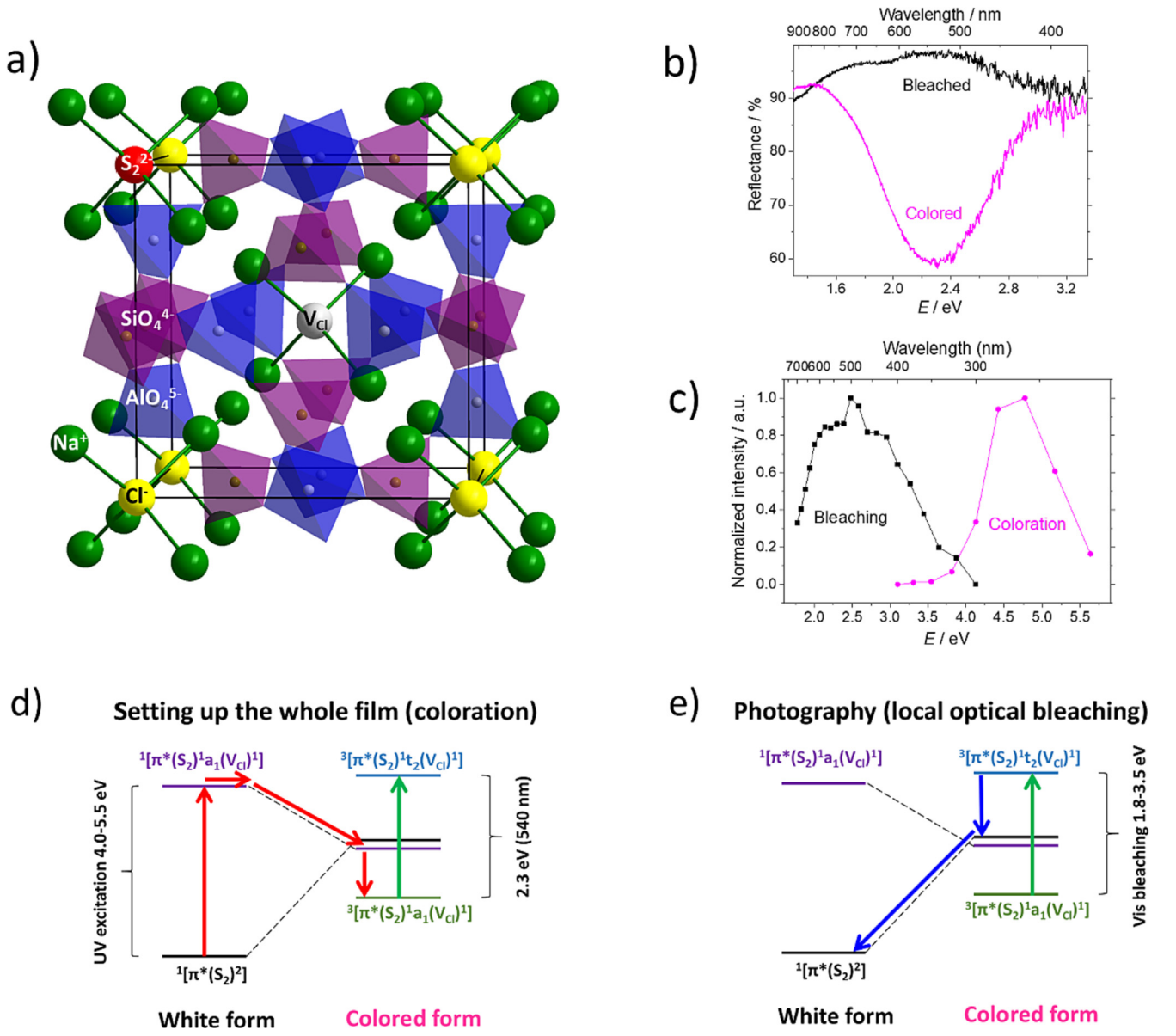

Fig. 13. (a) Unit cell of hackmanite with one chloride replaced by disulfide. (b) Reflectance spectrum of hackmanite film in its white (bleached) and colored state. (c) Tenebrescence bleaching and excitation (coloration) spectra for hackmanite film. (d) Mechanism of coloration and (e) mechanism of bleaching. For more information on the states involved, please see [38].

states involved in the mechanism as reported in [38] are presented in Fig. 13e. The thermal bleaching would require temperatures of ca. 100 °C as has been reported earlier [8,27].

For application in photography, the hackmanite film was first colored by using the 9-W UV lamp at 254 nm (Fig. 14a). The colored film was placed on the inside back wall of the camera (Fig. 14b and c). The front lens element focuses the image on the hackmanite film, which then bleaches position-sensitively. The magnitude of bleaching at each position of the film depends on the dose of white light received.

Conclusions

We have shown for the first time that hackmanite can be synthesized in industrial scale quantities, specifically 100 g and 1 kg, simply by mixing the starting materials in a bag and putting them into an industrial furnace for synthesis. Considering that hackmanites' tenebrescent and luminescent properties are based on lattice defects created with the help of a reducing gas sphere, such scale-up from the 1-g laboratory scale cannot be considered a trivial task. Washing the synthetic hackmanite with water purifies it by removing excess NaCl and results in phase purity. The 100 g batch that was synthesized with a protective lid on top of the reaction vessel had higher purity in terms of unreacted NaCl and Fe impurities and better overall optical properties. Thus, using a lid was shown to be beneficial. The surface layer of the Hack 1 kg, which was not protected with a lid, showed greatly weakened luminescence properties due to iron contamination. The bulk inside the Hack 1 kg batch showed the best luminescence properties, and Hack 100 g performed slightly more poorly in this aspect due to the measured samples, in spite of the lid, containing both the surface layer and bulk. Tenebrescence, on the other hand, was worse in the Hack 1 kg sample, a fact that can be explained by the delicate interplay of energy-requiring optical properties: the tenebrescence and luminescence or persistent luminescence features all exploit incident UV photons. Hence, the more UV pho-

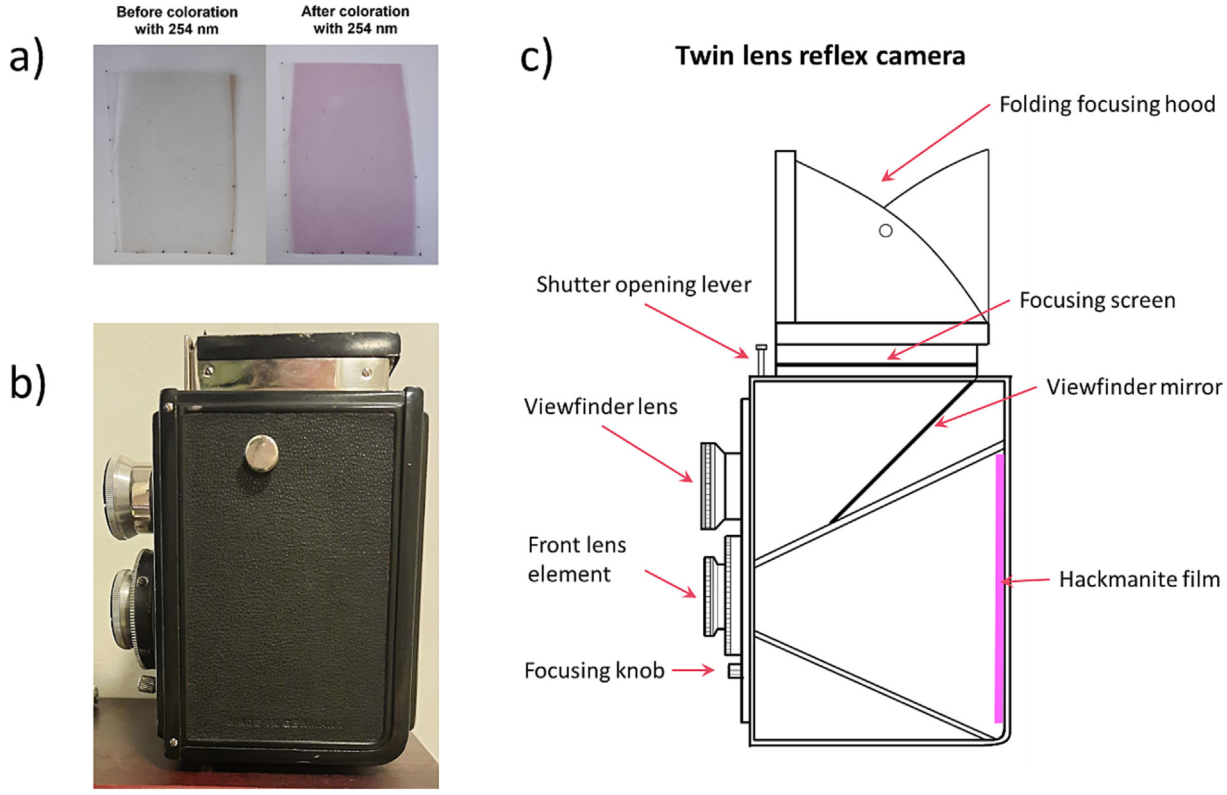

Fig. 14. (a) Hackmanite film before and after coloration with 254 nm. (b) Photo and (c) schematic drawing of the camera used.

tons involved in exciting luminescence, the less free photons are available for the tenebrescence feature.

As for the practical applications of the upscaling, in the textile industry it has been shown that 10% of hackmanite can be incorporated into cellulose dope without losing its important properties [17]. This means that e.g. 1 kg of this kind of intelligent fabric requires 100 g of hackmanite, which is 100 times more than the average laboratory synthesis produces. Thus, our demonstration of an up-scaled synthesis is an important step in making applications such as this commercially viable.

We have shown for the first time that hackmanite can be used in photography as a reusable, low-cost, ultra-long exposure film that requires no specialized methods for reading the image, after which the image can be erased with a low-cost UV lamp, and the film reused. The novel invention can be used in its current state as a way for long-exposure photography, which is an artistic method where any movement can be faded in the scene, i.e. for making running water to have a silky smooth-looking surface, and also to make a bustling city center look like it is entirely free of people, only showing stationary objects. However, since the photographic film is not optimized in any way, further examination is desirable in this matter, especially with respect to making the exposure time faster without a coloration depth trade-off or losing other desirable properties.

CRediT authorship contribution statement

Sami Vuori: Investigation, Data curation, Formal analysis, Writing – original draft, Writing – review & editing. **Hannah Byron:** Investigation, Writing – review & editing. **Isabella Norrbo:** Investigation, Writing – review & editing. **Minnea Tuomisto:** Investigation, Writing – review & editing. **Mika Lastusaari:** Investigation, Conceptualization, Funding acquisition, Project administration, Supervision, Writing – review & editing.

Declaration of Competing Interest

The authors declare the following financial interests/personal relationships which may be considered as potential competing interests: [Mika Lastusaari reports financial support was provided by Business Finland. Sami Vuori reports financial support was provided by Business Finland. Hannah Byron reports financial support was provided by Business Finland. Isabella Norrbo reports financial support was provided by Business Finland. Minnea Tuomisto reports financial support was provided by Business Finland.]

Acknowledgements

The authors want to thank Business Finland (project #6479/31/2019) for funding, Shukri Mahamuud for gathering and indexing the 19 samples from each batch and conducting measurements, Dr. Anssi Peuronen for his XRD expertise, and Hilamet Oy's Markus Mäkelä, Jouni Rahkola, and Matti Rahkola for their hospitality and vast technical knowledge.

Appendix A. Supplementary material

Supplementary data to this article can be found online at https://doi.org/10.1016/j.jiec.2022.12.043.

References

[1] J.W. Anthony, R.A. Bideaux, K.W. Bladh, M.C. Nichols, Handbook of Mineralogy, Mineralogical Society of America, Chantilly, VA, 2001.
[2] W.A. Deer, R.A. Howie, W.S. Wise, J. Zussman, Rock-forming minerals - framework silicates, 2nd ed., The Geological Society, 2004.
[3] O.I. Lee, Am. Mineral. 21 (1936) 764–776.
[4] D.B. Medved, Am. Mineral. 39 (1954) 615–629.
[5] H.D. Miser, J.J. Glass, Am. Mineral. 26 (1941) 437–445.
[6] R.D. Kirk, Am. Mineral. 40 (1955) 22–31.

[7] C. Agamah, S. Vuori, P. Colinet, I. Norrbo, J.M. de Carvalho, L.K. Okada Nakamura, J. Lindblom, L. van Goethem, A. Emmermann, T. Saarinen, T. Laihinen, E. Laakkonen, J. Lindén, J. Konu, H. Vrielinck, D. van der Heggen, P.F. Smet, T. Le Bahers, M. Lastusaari, Chem. Mater. 32 (2020) 8895–8905.
[8] I. Norrbo, A. Curutchet, A. Kuusisto, J. Mäkelä, P. Laukkanen, P. Paturi, T. Laihinen, J. Sinkkonen, E. Wetterskog, F. Mamedov, T. Le Bahers, M. Lastusaari, Mater Horiz. 5 (2018).
[9] S. Vuori, P. Colinet, I. Norrbo, R. Steininger, T. Saarinen, H. Palonen, P. Paturi, L. C.V. Rodrigues, J. Göttlicher, T. Le Bahers, M. Lastusaari, Adv Opt Mater. 9 (2021) 2100762.
[10] S. Vuori, P. Colinet, J.-P. Lehtiö, A. Lemiere, I. Norrbo, M. Granström, J. Konu, G. Ågren, P. Laukkanen, L. Petit, A.J. Airaksinen, L. van Goethem, T. Le Bahers, M. Lastusaari, Mater Horiz. (2022).
[11] H. Byron, I. Norrbo, M. Lastusaari, J. Alloy. Compd. 872 (2021).
[12] I. Norrbo, P. Gluchowski, P. Paturi, J. Sinkkonen, M. Lastusaari, Inorg. Chem. 54 (2015) 7717–7724.
[13] L.T. Todd, E.F. Farrell, Process for preparing cathodochromic sodalite, 1974.
[14] E.F. Williams, W.G. Hodgson, J.S. Brinen, J. Am. Ceram. Soc. 52 (1969) 139–144.
[15] J.A. Armstrong, M.T. Weller, Chem. Commun. (2006) 1094–1096.
[16] E.R. Williams, A. Simmonds, J.A. Armstrong, M.T. Weller, J. Mater. Chem. 20 (2010) 10883–10887.
[17] W. Fang, E. Sairanen, S. Vuori, M. Rissanen, I. Norrbo, M. Lastusaari, H. Sixta, ACS Sustain. Chem. Eng. 9 (2021) 16338–16346.
[18] "KARKAISU JA PÄÄSTÖ | HILAMET OY | Kauhava | Hämeenkyrö", (n.d.). https://www.hilamet.fi/karkaisu-ja-paeaestoe (accessed September 25, 2022).
[19] Y. Jin, Y. Hu, Y. Fu, L. Chen, G. Ju, Z. Mu, J. Mater. Chem. C Mater. 3 (2015) 9435–9443.
[20] Q. Zhang, Y. Zhang, H. Sun, Q. Sun, X. Wang, X. Hao, S. An, J. Eur. Ceram. Soc. 37 (2017) 955–966.
[21] Y. Jin, Y. Hu, L. Yuan, L. Chen, H. Wu, G. Ju, H. Duan, Z. Mu, J. Mater. Chem. C Mater. 4 (2016) 6614–6625.
[22] S. Cao, F. Gao, J. Xu, J. Zhu, Q. Chen, Y. Guo, L. Li, J. Liu, T. Gao, E. Pawlikowska, M. Szafran, G. Cheng, J. Eur. Ceram. Soc. 39 (2019) 5260–5266.
[23] M. Akiyama, H. Yamada, K. Sakai, J. Ceram. Soc. Jpn. 119 (2011) 338–341.
[24] Y. Ren, Z. Yang, Y. Wang, M. Li, J. Qiu, Z. Song, J. Yu, A. Ullah, I. Khan, Sci. China Mater. 63 (4) (2020) 582–592.
[25] Y. Jin, Y. Lv, C. Wang, G. Ju, H. Wu, Y. Hu, Sens. Actuators B Chem. 245 (2017) 256–262.
[26] "The Periodic Table of Endangered Elements - American Chemical Society", (n.d.). https://www.acs.org/greenchemistry/research-innovation/endangered-elements.html (accessed December 6, 2022).
[27] P. Colinet, H. Byron, S. Vuori, J.-P. Lehtiö, P. Laukkanen, L. van Goethem, M. Lastusaari, T. Le Bahers, PNAS 119 (2022).
[28] I. Norrbo, P. Gluchowski, I. Hyppänen, T. Laihinen, P. Laukkanen, J. Mäkelä, F. Mamedov, H.S. Santos, J. Sinkkonen, M. Tuomisto, A. Viinikanoja, M. Lastusaari, ACS Appl. Mater Interfaces. 8 (2016) 11592–11602.
[29] S. Abhinay, R. Mazumder, A. Seal, A. Sen, J. Eur. Ceram. Soc. 36 (2016) 3125–3137.
[30] K. Pigmente, "Sodalite Material Safety Data Sheet", (2012) 1–4. http://www.kremer-pigmente.de, (accessed September 28, 2022).
[31] M. Gaft, R. Reisfeld, G. Panczer, Modern Luminescence Spectroscopy of Minerals and Materials, 2nd ed., Springer International Publishing, 2015.
[32] Kodak Alaris Holdings Limited, "Kodak Alaris Annual Report & Accounts", (2021) 22–22. https://www.kodakalaris.com/getmedia/c920a71f-c9dd-4140-ab56-4c27e7866bc2/FY21-Accounts-Final-and-Signed.pdf.aspx (accessed September 27, 2022).
[33] T.R. Keenan, Kirk-Othmer Encyclopedia Chem. Technol 12 (2000).
[34] I.N. Gorokhovskii, T.M. Levenberg, Obshchaia sensitometriia: Teoriia i praktika, 1963. https://encyclopedia2.thefreedictionary.com/Hurter-Driffield+curves (accessed September 29, 2022).
[35] G.K. Burgess, Scientific Papers of the Bureau of Standards - United States. National Bureau of Standards, Department of Commerce, US, Washington, 1923.
[36] R.D. Portugal, B.F. Svaiter, Mind. Mach. 21 (1) (2010) 73–81.
[37] I. Hassan, S.M. Antao, J.B. Parise, Am. Mineral. 89 (2004) 359–364.
[38] A. Curutchet, T. Le Bahers, Inorg. Chem. 56 (2017) 414–423.